Electronic Supplementary Material (ESI) for Materials Horizons.

Supplementary Materials for

Stress-Localized Durable Icephobic Surfaces

Peyman Irajizad[1], Abdullah Al-Bayati[1], Bahareh Eslami[1], Taha Shafquat[1], Masoumeh Nazari[1], Parham Jafari[1], Varun Kashyap[1], Ali Masoudi[1], Daniel Araya[1,2] and Hadi Ghasemi[1*]

[1]Department of Mechanical Engineering, University of Houston, Houston, TX 77204-4006, USA

[2]Senior Aerospace Engineer, Johns Hopkins University Applied Physics Laboratory

*Correspondence to: hghasemi@uh.edu

S1. Standard method for ice adhesion measurement

We have developed a standard procedure for measurement of ice adhesion. The lack of this standard method in literature has resulted in a wide range of reported ice adhesion values for the same sample. For example, the reported values of ice adhesion for PDMS varies in the range of 100-800 kPa[1–3].

Let's consider a rigid ice phase attached to an elastomer as shown in **Fig. S1**. If a force is applied in the plane of ice-coating, the ice would only slide with no detachment from the surface. However, if the force is applied at a plane higher than the interface, the ice would detach at a critical stress. The adhesion on elastomers depends on the applied shear rate and the geometry of the experimental setup (i.e. a, l, and h). Note that at small shear rates, the ice can slide on the surface for a long distance with no detachment. Thus, it is required to find a shear rate at which the critical shear stress is achieved and fracture occurs at the interface. This critical shear rate depends on the shear modulus of the elastomer. The critical shear rate is an inverse function of shear modulus[4]. Through studies of different elastomers with shear modulus in the range of 0.5 MPa-100 MPa and thickness of $300 \pm 20\,\mu m$, we found that the upper limit of critical shear rate for the measurement of ice adhesion is 0.1 mms^{-1}. This shear rate is consistent with the shear rate reported by Meuler et al.[2] In addition to shear rate, we should define the values of geometrical parameters for a standard test. As discussed by Chaudhury et al.[4], adhesion of a rigid solid on an isotropic elastomer is written as

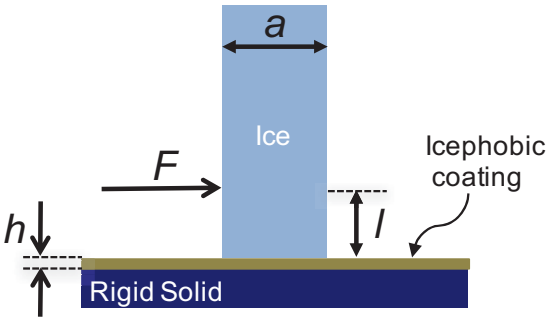

Figure S1: Schematic of the experimental approach to measure ice adhesion.

$$\sigma_s \sim \left(\frac{a}{l}\right)\sqrt{\frac{W_a G}{h}} \tag{1}$$

In the derivation of this formula, lubrication approximation of the Stokes equation is used to determine the hydrostatic pressure field in the elastomer. This approximation is valid as long as the a and h satisfy $\frac{a}{h} \gg 1$. Thus, in the standard experimental procedure, we define the value of a as 15 mm and the value h to 300 μm. Furthermore, in the derivation of **Eq. 1**, linear relation between the vertical displacement of the ice and horizontal length scale is considered. This linear relation requires $l/a \ll 1$. Thus, we define the value of l as 3 mm in all the experiments. In summary, the parameters for standard ice adhesion measurement are tabulated in **Table S1**. This standard method provides a rational and unified approach to compare ice adhesion of coatings reported by various laboratories with the same metrics.

Table S1: Parameters of standard procedure for ice adhesion measurements.

Surface temperature	Shear rate	a	h	l
-25 °C	0.1 mms^{-1}	15 mm	300 μm	3 mm

S2. Stress localization in viscoelastic materials

As shown in **Fig. S1**, the force, F, applied at a plane slightly above the interface generates an external torque leading to a normal stress at the interface, $F.l = a\int \sigma_n\, x\, dx$, where a denotes the dimension of ice, σ_n the normal stress at the interface, and x is the horizontal axis. Note that $F = a^2\sigma_s$, where σ_s is the adhesion stress of the interface (i.e. $\sigma_s \sim \left(\frac{a}{l}\right)\sigma_n$). It has been shown by Chaudhury et al.[4] that the elastic instability at the interface of a rigid body and an elastomer is responsible for the crack formation and detachment of the solid from the surface. The strain energy per unit area of the elastomer can be simplified by taking into account the equation of continuity and is written as

$$U_T \sim Gh\,\delta^2\,[\frac{\lambda}{h^2} + \frac{1}{\lambda}]^2 \tag{2}$$

where G denotes shear modulus of the elastomer, h is the thickness of the elastomer, δ is the amplitude of perturbation of the elastomer film and λ is the wavelength of the elastic waves at the interface. Minimization of this energy with respect to λ results in $\lambda \sim h$. By taking the derivate of the strain energy with respect to δ, one finds normal stress at the interface written as $\sigma_n \sim G\,\delta/h$. The total energy of the elastomer-ice system per unit width (U) is expressed as

$$U = \left(\int_0^a \int_0^{\delta^*} \sigma_n\, d\delta\, dx\right) - W_a a \tag{3}$$

where δ^* denotes the maximum displacement at the interface caused by the instability and W_a is the work of adhesion. In this formulation on the right-hand side, the first term represents stored elastic energy in the elastomer and the second term represents the surface energy. The critical stress (i.e. detachment stress) is found by setting the derivate of total energy with respect to maximum displacement. By using the definition of σ_n, one finds,

$$W_a \sim \frac{G{\delta^*}^2}{h} \tag{4}$$

For a uniform elastomer with isotropic properties and linear correlation of vertical displacement with respect to a, one finds that the adhesion stress at the interface is equivalent to

$$\sigma_s \sim \left(\frac{a}{l}\right)\sqrt{\frac{W_a G}{h}} \tag{5}$$

However, for viscoelastic materials including two phases (or can be more) denoted as phase I and phase II, two modifications to above formulation should be taken into account.
First, the properties should be modified to composite structure properties written as[5]

$$G_m = G_{\mathrm{I}}\,[\frac{1 - B_i\,\psi\,\varphi_{\mathrm{II}}}{1 + A_i\,B_i\,\varphi_{\mathrm{II}}}] \tag{6}$$

where

$$B_i = \frac{\frac{G_{\mathrm{I}}}{G_{\mathrm{II}}} - 1}{\frac{G_{\mathrm{I}}}{G_{\mathrm{II}}} + A_i} \tag{7}$$

and

$$A_i = (k-1)^{-1} \tag{8}$$

where G_{I} denotes the shear modulus of the matrix (Phase I), G_{II} is the shear modulus of the second phase (Phase II), k the Einstein coefficient and $\psi = 1 + \frac{(1-\varphi_m)}{{\varphi_m}^2}\,\varphi_{\mathrm{II}}$, where φ_m is the maximum packing fraction of the dispersed phase and φ_{II} is the volumetric fraction of phase II. Furthermore, work of adhesion of the these viscoelastic material is written as

$$\overline{W_a} = \varphi_{\mathrm{I}} W_{a\mathrm{I}} + \varphi_{\mathrm{II}} W_{a\mathrm{II}} \tag{9}$$

where $W_{a\mathrm{I}}$ denotes the work of adhesion of the rigid matrix and $W_{a\mathrm{II}}$ is the work of adhesion of the Phase II.

The other modification to this formulation is the stress localization effect, which needs to be rigorously formulated. For one-phase elastomeric material, the elastic instability at the solid-elastomeric interface results into normal force, σ_n. Once the stored energy by this normal force is balanced by the work of adhesion, W_a, the crack propagates at the interface for detachment of solid from the elastomer. In other words,

$$\mathrm{U} = {\sigma_n}^2 \frac{h\,a^2}{G} = W_a\,a^2 \tag{10}$$

Considering $\sigma_s \sim \left(\frac{a}{l}\right)\sigma_n$, this equation results in Eq. 5. However, in the micro/nano elastomeric materials, with minimal force, the solid is detached from phase II as they have much lower shear modulus than the matrix, phase I. This fact is demonstrated in Fig. 5b in the manuscript. The formed defects at the interface induce a local stress and the elastic energy stored around this defect is equal to $G\,r^3$, where r is the characteristic length of the defect. Major portion of the induced elastic energy around these defects leads to propagation of crack and possibly a portion of it is dissipated in the elastomer. The localized elastic energy, U_L, to open the crack with length of r is written as

$$\mathrm{U}_L = {\sigma_s}^2 \frac{h\,r^2}{G} = {\sigma_s}^2 \frac{h\,a^2}{G} f(\varphi_{\mathrm{II}}) \tag{11}$$

where $f(\varphi_{\mathrm{II}})$ denotes the fraction of phase II. We should emphasize that the crack propagation in the phase I is dominated by normal stress energy while this energy release in the crack front is dominated by shear strain energy. Thus, the total released energy can be written as linear combination of elastic energy of phase I and the local elastic energy induced by phase II.

$$\mathrm{U}_t = \alpha \mathrm{U}_M + \beta \mathrm{U}_L \tag{12}$$

where α and β are the proportionality factors. Once this energy is balanced by the work of adhesion, the crack is propagated and leads to detachment of solid from the material. That is,

$$\mathrm{U}_t = \alpha \left({\sigma_n}^2 \frac{h\,a^2}{G}\right) + \beta \left({\sigma_s}^2 \frac{h\,a^2 f(\varphi_{\mathrm{II}})}{G}\right) = W_a\,a^2 \tag{13}$$

Having $\sigma_s \sim \left(\frac{a}{l}\right)\sigma_n$, the equation could be rearranged and written as

$${\sigma_s}^l = \frac{1}{\sqrt{\alpha + \beta\, f(\varphi_{\mathrm{II}})\frac{a^2}{l^2}}} \left(\frac{a}{l}\right) \sqrt{\frac{\overline{W_a}\,G_m}{h}} \tag{14}$$

or by defining a stress localization function as $g(\varphi_{\mathrm{II}}) = \frac{1}{\sqrt{\alpha+\beta\, f(\varphi_{\mathrm{II}})\frac{a^2}{l^2}}}$, the equation is written as

$$\sigma_s{}^{L} = g(\varphi_{\mathrm{II}}) \left(\frac{a}{l}\right) \sqrt{\frac{\overline{W_a}\, G_m}{h}} \tag{15}$$

The stress localization function, $g(\varphi_{\mathrm{II}})$, results from localized energy around phase II in the material. As the shear modulus of the second phase is small, we neglected the stored strain energy in this phase compared to the phase I (i.e. the matrix). The new formulation allows us to tune the value of G_m, $\overline{W_a}$ and $g(\varphi_{\mathrm{II}})$ to minimize the adhesion stress with no compromise on the durability of the structure. Note that mechanical durability of the stress-localized viscoelastic material is mainly governed by phase I.

S3- Development of stress-localized icephobic materials

Properties of the elastomer used as phase I are tabulated in **Table S2**.

Table S2: Material properties of RTV-1 Silicon rubber

Property	Inspection Method	Value
Elongation at break	DIN 53504 S1 / ISO 37	500 %
Hardness Shore A	DIN 53 505 / ISO 868	30
Tensile strength	DIN 53504 S1 / ISO 37	8 N/mm²
Viscosity, dynamic at 20 °C	DIN EN ISO 3219	300000 mPa.s
Density at 23 °C in water	DIN EN ISO 1183-1 / ISO 2781	1.1 g/cm³
Tear strength	ASTM D 624	13.5 N/mm

Phase II, organogel particles, consists of tuned liquid organic phases (non-crosslinked components in the gel matrices) entrapped within a solid phase (three-dimensionally crosslinked gel network). The procedure for development of these organogels are as follow: 10 mL of Sylgard 184 base was mixed with 1 mL of Sylgard 184 curing agent. 100 mL of an organic liquid (i.e. Polydimethylsilaxone) was added to this mixture. The solution was then vigorously mixed to obtain a homogeneous solution. The precursor sample was heated at 100 °C for 4 hrs in a petri dish. The final product is a non-syneresis oreganogel. Non-syneresis property of organogel comes from miscibility of silicone oil with PDMS before and after gelation[6].

Once phase II was developed, it was crushed in the presence of silicon oil for ten minutes to avoid aggregation of gel particles. The solution was filtered to remove excess oil. The final product is a batch of gel particles with dimension in the range of 2-20 µm. The particles were

mixed with the elastomer in a pre-defined concentration. The solution was diluted with a solvent, Hexamethyldisilaxane, to reduce viscosity for spraying on a surface.

For a substrate with given surface area, we measured volume of the coating material needed for thickness of $300 \pm 20\ \mu m$. The coating material was diluted with the solvent to uniformly spread over the substrate. After curing, thickness of the sample was double-checked with a caliper to ensure uniform thickness.

The surface roughness of icephobic sample DI-25 is measured through scanning probe microscopy (SPM, Bruker Multimedia 8) as shown in **Fig. S2**. The average roughness of sample is 18 nm.

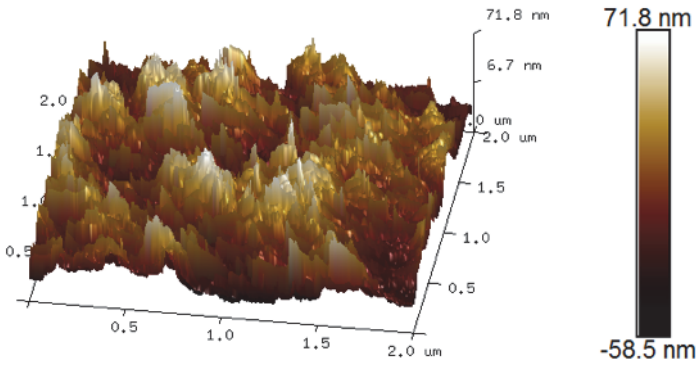

Figure S2: Roughness of icephobic sample DI-25 measured through SPM

S4- Ice adhesion measurements

As discussed above, we developed a standard procedure to examine ice adhesion on various materials. Standard protocol has been followed for all the measurements. The schematic of experiments is shown in **Fig. S3**. The test chamber was cooled at a rate of ~2 °C/min to the target temperature. Temperature of the cooling plate was monitored using a thermocouple on top of the plate.

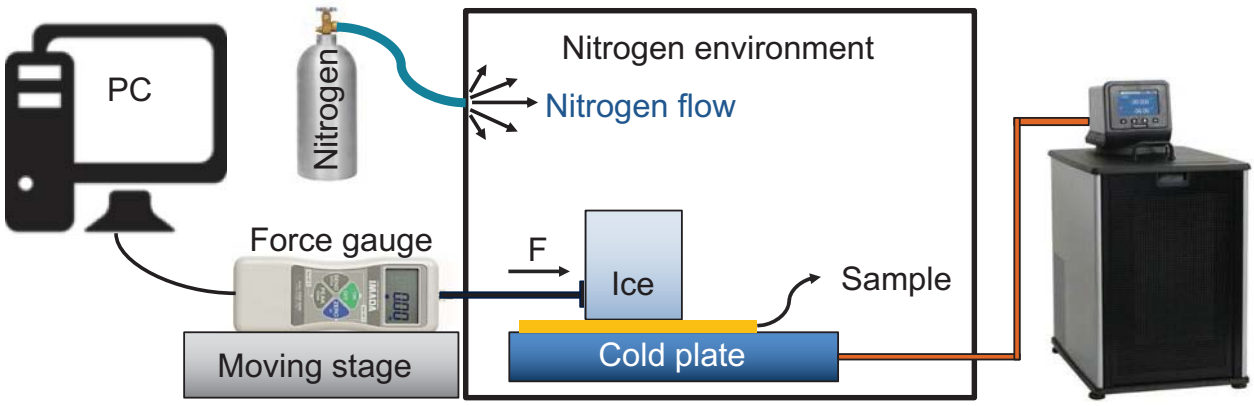

Figure S3: Schematic of the setup for ice adhesion measurements.

The icephobic sample was placed on the cooling plate. A square acrylic cuvette with dimension of 15 mm by 15 mm was fabricated with laser cutter with an accuracy of 100 µm. The edges of cuvette were coated with Silane in order to achieve low surface energy and minimize adhesion of cuvette to the icephobic surface. This step minimizes the errors in ice adhesion measurements. The cuvette was filled with deionized water and was allowed to freeze for 1 hr. Ice column encased in acrylic columns and adhered to the test samples. The force required to detach each ice column was measured by propelling the 4 mm diameter probe of a force transducer (Imada, model DS2-110) to the side of the ice columns at a constant velocity of 0.1 mm/s. The probe velocity was controlled using a syringe pump. The center of probe was located at 3 mm above the material surface. The measured maximum force at break was converted into ice adhesion strength by dividing by the known cross-sectional area (2.25 cm^2) of the ice-substrate interface. The entire experiment was conducted in a low-humidity nitrogen atmosphere to minimize frost formation on the samples and the test apparatus.

S5- Icing/deicing procedure

For these experiments, once the ice column was detached from the substrate, a new cuvette was placed on the sample and the procedure for ice formation was repeated. After complete formation of ice column, standard procedure was followed to measure ice adhesion. For the same sample, we conducted these experiment up to 100 times during a week to demonstrate consistency of ice adhesion on these icephobic surfaces.

S6- Shear flow experiments

For these experiments, icephobic material of DI-67 was coated on a glass substrate through spraying. The sample was left to cure for 24 hr. The ice adhesion on the sample was measured through the standard protocol. Next, the coated glass substrate was placed in a tube and initially was exposed to shear flow of water as shown in **Fig. S4a**. The sample was left under high shear flow for one month. After this time period, the ice adhesion on the sample was re-measured.
The same sample was moved to another setup and was exposed to shear flow of air with Reynolds number of 30000 for one month as shown in **Fig. S4b**. The ice adhesion on the samples was re-measured after this experiment.

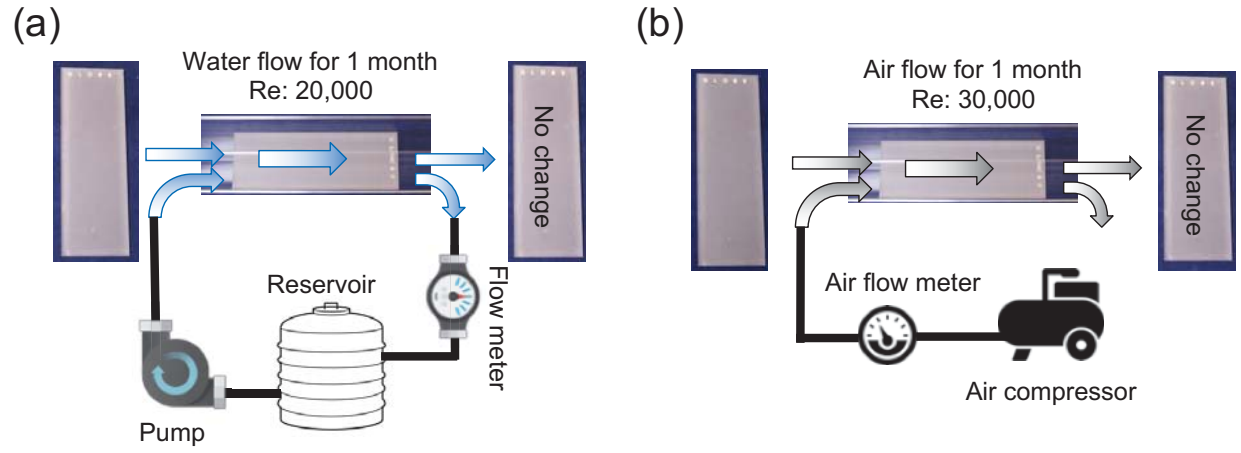

Figure S4: (a) schematic of setup to determine durability of stress-localized samples under high water shear flow. (b) schematic of setup to examine durability of icephobic samples under long-term air flow.

S7- Durability of pure phase II

We developed a sample of pure phase II. The sample was placed on the Taber abrasion platform to measure its mechanical durability. Even with the load of 1 N, the abrader pin penetrates through the sample in one motion and touches the substrate. No conclusive abrasion test could be conducted on this sample. Note that for mechanical durability tests, 1000 cycle of abrasion is required.

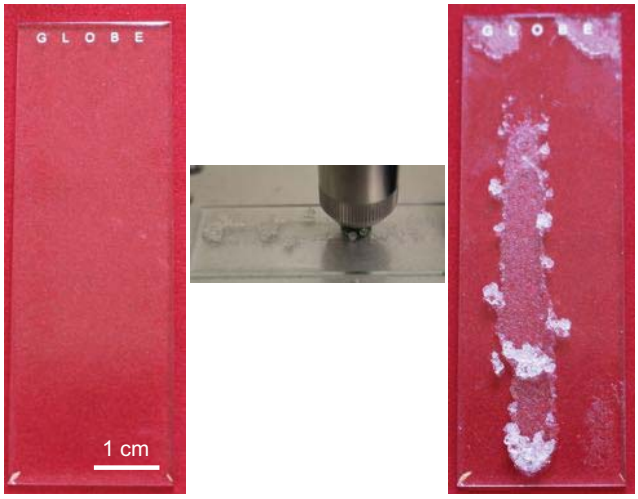

Figure S5: Mechanical durability of pure phase II. Even with a minimal weight, 1 N, the abrader pin penetrates through the sample and touches the underlying substrate. No conclusive abrasion test can be conducted.

S8- Aerodynamics of airfoil

The experimental setup is an aluminum wing with a length of 11 inches long and chord length of 1.76 inches, **Fig. S6**. The wing cross-section is very close to a NACA 6415 airfoil[7]. Before conducting any experiments, the lift and drag coefficients were estimated for different angles of attack using XFOIL[8], a program developed to analyze subsonic isolated airfoils. XFOIL analyzes the 2D airfoil profile of a NACA 6415 under viscous flow conditions with a Reynolds number of 90,000 and a Mach number of 0.09 to compute the lift and drag characteristics of the airfoil.

Figure S6: NACA 6415 Airfoil Profile

The mounting system was designed using Autodesk Inventor and was tailored specifically for use with the NACA 6415 cross-section and the 6-Axis load cell. The mounting system consisted of an airfoil mount and two circular plates as part of the load cell mounts, one of which was fixed to the base of the wind tunnel and the other was fixed to the bottom of the load cell. The two load cell plates were designed in such a way that the top plate could rotate on top of the bottom plate, with increments of 1°, covering the complete 360° range. This design feature was used to change the angle of attack of the wing section attached to the load cell. The plates were also designed to have 360 holes so that the plates could be pinned to hold the testing system at a certain angle of attack. After the CAD drawing was made, the mounting system was 3D-printed using PLA (Polylactic Acid) filament with a 100 infill to provide structural rigidity. Each wing section was

attached to a 6-Axis load cell in the wind tunnel, which in turn was attached to the base of the wind tunnel. The 6-Axis load cell measures the forces and torques acting on the surface of the load cell and has a left-handed coordinate system. The wings were tested at a constant wind speed of 17 m/s, so as to match the conditions used in XFOIL. The forces and torques acting on the wing were measured simultaneously by the load cell for a given angle of attack. The force and torque measurements were used to determine the 2D drag and lift curves for the airfoil, with and without the icephobic coating.

S9- Measurement of work of adhesion and shear modulus

Work of adhesion on a surface is written as

$$W_a = \gamma^w(1 + \cos\theta) \quad (16)$$

Where γ^w denotes surface tension of liquid (i.e. water) at -25 °C and θ is the contact angle of sessile droplet on the surface. The value of surface tension of water was extrapolated from the surface tension dependence on temperature. For temperature of -25 °C, this value is 79 mN/m.
As shown in **Fig. S7**, we determined contact angle of water on various samples and consequently determined work of adhesion.

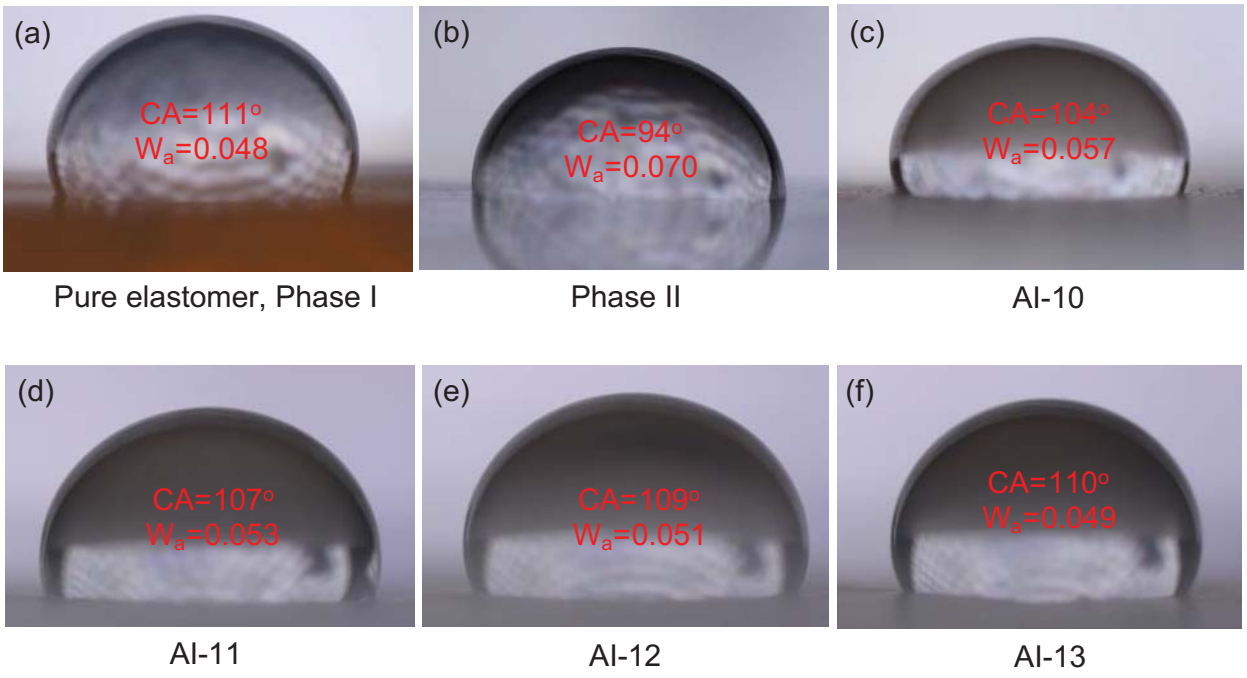

Figure S7: (a)-(f) Measured contact angle and consequently work of adhesion on different stress-localized icephobic samples.

The shear modulus of the developed icephobic samples were measured through Dynamic Mechanical Analyzer (TA Instruments, DMA Q800) at ambient temperature (i.e. 23 °C). The measured values are tabulated in **Table S3**. The dependence of shear modulus of elastomers on temperature is reported by Lotters et al.[9] The curve indicates that the shear modulus varies by

approximately 20% between -25 °C to 23 °C. This results in ~ 10% error in ice adhesion values which is within the error bar of our measurements.

Table S3. Surface and mechanical properties of stress-localized icephobic samples

	Phase I	Phase II	DI-67	DI-50	DI-33	DI-25
$\overline{W_a}$ (mN/m)	48 ± 3	70 ± 3	57 ± 3	53 ± 3	51 ± 3	49 ± 3
G_m (MPa)	3.5 ± 0.5	NA	0.6 ± 0.5	0.9 ± 0.5	1.4 ± 0.5	1.8 ± 0.5

References

1. Wang, C., Fuller, T., Zhang, W. & Wynne, K. J. Thickness dependence of ice removal stress for a polydimethylsiloxane nanocomposite: Sylgard 184. *Langmuir* **30,** 12819–12826 (2014).
2. Meuler, A. J. *et al.* Relationships between water wettability and ice adhesion. *ACS Appl. Mater. Interfaces* **2,** 3100–10 (2010).
3. Susoff, M., Siegmann, K., Pfaffenroth, C. & Hirayama, M. Evaluation of icephobic coatings - Screening of different coatings and influence of roughness. *Appl. Surf. Sci.* **282,** 870–879 (2013).
4. Chaudhury, M. K. & Kim, K. H. Shear-induced adhesive failure of a rigid slab in contact with a thin confined film. *Eur. Phys. J. E* **23,** 175–183 (2007).
5. Nielsen, L. E. Generalized equation for the elastic moduli of composite materials. *J. Appl. Phys.* **41,** 4626–4627 (1970).
6. Urata, C., Dunderdale, G. J., England, M. W. & Hozumi, A. Self-lubricating organogels (SLUGs) with exceptional syneresis-induced anti-sticking properties against viscous emulsions and ices. *J. Mater. Chem. A* **3,** 12626–12630 (2015).
7. Fazil, J. & Jayakumar, V. Investigation of airfoil profile design using reverse engineering Bezier curve. *J. Eng. Appl. Sci.* **6,** 43–52 (2011).
8. Drela, M. & Youngren, H. *XFOIL 6.94 user guide*. (2001).
9. Lötters, J. C., Olthuis, W., Veltink, P. H. & Bergveld, P. The mechanical properties of the rubber elastic polymer polydimethylsiloxane for sensor applications. *J. Micromechanics Microengineering* **7,** 145–147 (1997).